Supplemental Material S1

1 Computation model in detail

The transient point contact TEHL model consists of the following equations.

Reynolds equation with squeeze term:

$$\frac{\partial}{\partial x}\left(\frac{\rho h^3}{12\eta}\frac{\partial p}{\partial x}\right)+\frac{\partial}{\partial y}\left(\frac{\rho h^3}{12\eta}\frac{\partial p}{\partial y}\right)=u_s\frac{\partial(\rho h)}{\partial x}+\frac{\partial(\rho h)}{\partial t} \tag{S(1)}$$

The x and y are the coordinate axes, ρ is the density, η is the viscosity, p is the pressure distribution, h is the film thickness distribution, u_s is the entrainment speed, and t is the time.

Film thickness equation:

$$h(x,y,t)=h_0(t)+\frac{x^2}{2R_x}+\frac{y^2}{2R_y}+r(x,y,t)+v(x,y,t) \tag{S(2)}$$

where h_0 is the minimum undeformed gap, R_x and R_y are radii of curvature in x and y direction, r is the waviness of the upper body at time t, and v is the elastic deformation.

Elastic deformation equation:

$$v(x,y,t)=\frac{2}{\pi E_e}\iint_{\Omega}\frac{p(\xi,\zeta,t)}{\sqrt{(x-\xi)^2+(y-\zeta)^2}}d\xi d\zeta \tag{S(3)}$$

where E_e is the equivalent Young's modulus.

Load balance equation:

$$w=\iint_{\Omega}p(x,y,t)dxdy \tag{S(4)}$$

where w is the applied load.

The flash temperature distribution is calculated by the moving-point heat-source integration method [1, 2]. The thermal deformation of surfaces is ignored following the models of He et al. [3]. A heat flux $q(x,y,t)\in\Omega_q$ assigns to the surface of a half-space solid and moves with speed V along the X direction. The heat source $q(x',y',t')$ at point (x',y') and time t' will generate a temperature rise at point (x,y) and time t as follows:

$$dT=\frac{q(x',y',t')dx'dy'dt'}{4\rho_s c_s\left[\pi\alpha_s(t-t')\right]^{3/2}}\times\exp\left\{\frac{\left[(x-x')-V(t-t')\right]^2+(y-y')^2}{4\alpha_s(t-t')}\right\} \tag{S(5)}$$

where ρ_s is the density of the solid, c_s is the specific heat of the solid, α_s is the thermal

diffusivity of solid. Therefore, the total temperature rise during the period $(0,t)$ should be,

$$\Delta T(x,y,t)=\int_0^t\iint_{\Omega_q}\frac{q(x',y',t')dx'dy'dt'}{4\rho_s c_s\left[\pi\alpha_s(t-t')\right]^{3/2}}\times\exp\left\{\frac{\left[(x-x')-V(t-t')\right]^2+(y-y')^2}{4\alpha_s(t-t')}\right\} \quad \text{S(6)}$$

In EHL, friction heat is assumed to occur in the middle layer ($z=h/2$) of the lubricant. The frictional heat flux flows into the two surfaces. The temperature distribution along the film thickness direction changes linearly from the middle layer to the two surfaces. The temperature rise of the two surfaces is,

$$\Delta T_1(x,y,t)=\int_0^t\iint_{\Omega_q}\frac{q_1(x',y',t')dx'dy'dt'}{4\rho_1 c_1\left[\pi\alpha_{s1}(t-t')\right]^{3/2}}\times\exp\left\{\frac{\left[(x-x')-u_1(t-t')\right]^2+(y-y')^2}{4\alpha_{s1}(t-t')}\right\} \quad \text{S(7)}$$

$$\Delta T_2(x,y,t)=\int_0^t\iint_{\Omega_q}\frac{q_2(x',y',t')dx'dy'dt'}{4\rho_2 c_2\left[\pi\alpha_{s2}(t-t')\right]^{3/2}}\times\exp\left\{\frac{\left[(x-x')-u_2(t-t')\right]^2+(y-y')^2}{4\alpha_{s2}(t-t')}\right\} \quad \text{S(8)}$$

where $q_1(x',y',t')$ and $q_2(x',y',t')$ are the heat flux densities to surface 1 and 2, respectively. The heat flux results from friction as follows:

$$q(x,y,t)=\tau(x,y,t)|u_1-u_2| \quad \text{S(9)}$$

where $\tau(x,y,t)$ is the shear stress distribution. The $q_1(x',y',t')$ and $q_2(x',y',t')$ are calculated by the following equation:

$$q_1(x',y',t')=\left[1-f(x',y',t')\right]q(x',y',t')-q_c(x',y',t') \quad \text{S(10)}$$

$$q_2(x',y',t')=f(x',y',t')q(x',y',t')+q_c(x',y',t') \quad \text{S(11)}$$

where $f(x',y',t')\in[0,1]$ is the heat partition coefficients, $q_c(x',y',t')$ is the additional heat flux representing the bulk heat conduction. It satisfies

$$\begin{cases} if\left(q_c(x,y,t)=0\right)then\left(0\le f(x,y,t)\le 1\right) \\ if\left(q_c(x,y,t)>0\right)then\left(f(x,y,t)=1\right) \\ f\left(q_c(x,y,t)<0\right)then\left(f(x,y,t)=0\right) \end{cases}$$

Based on Fourier's Law, the temperature of two surfaces should satisfy

$$K_f\frac{T_m(x,y,t)-T_1(x,y,t)}{h(x,y,t)/2}=\left(1-f(x,y,t)\right)q(x,y,t)-q_c(x,y,t) \quad \text{S(12)}$$

$$K_f \frac{T_m(x,y,t) - T_2(x,y,t)}{h(x,y,t)/2} = f(x,y,t)q(x,y,t) + q_c(x,y,t) \quad \text{S(13)}$$

where K_f is the thermal conductivity of the fluid, T_m, T_1, and T_2 are the temperature of the middle layer, surface 1, and surface 2, respectively.

Eliminating the T_m by Equations S(14) and S(15) results in the matching equation of temperature:

$$\left[T_{2b} + \Delta T_2(x,y,t)\right] - \left[T_{1b} + \Delta T_1(x,y,t)\right] = \frac{\left(1 - 2f(x,y,t)\right)h(x,y,t)q(x,y,t)}{2K_f} - \frac{h(x,y,t)q_c(x,y,t)}{K_f} \quad \text{S(14)}$$

The viscosity and density of the lubricant are also functions of pressures and temperatures.

Viscosity-pressure-temperature equation:

$$\eta = \eta_0 \exp\left[\alpha p - \gamma(T - T_0)\right] \quad \text{S(15)}$$

where α is the pressure-viscosity coefficient, η_0 is the ambient viscosity value, γ is the temperature-viscosity coefficient, T_0 is the reference temperature.

Density-pressure-temperature equation:

$$\frac{\rho}{\rho_0} = 1 + \frac{0.6p}{1 + 1.7p} - \beta(T - T_0) \quad \text{S(16)}$$

where the unit of p is GPa, ρ_0 is the ambient density value, β is the temperature-density coefficient.

The shear stress distribution $\tau(x,y,t)$ is essential for calculating frictional heat and coefficient of friction. In a recent paper by the authors, a shear stress model reported by Bair et al. [4] was used. The same model is used in this work.

$$\tau = \tau_L\left(1 - e^{-\eta\dot{\gamma}/\tau_L}\right) \quad \text{S(17)}$$

$$\tau_L = \tau_{L0} + \gamma_L p_h \quad \text{S(18)}$$

where $\dot{\gamma}$ is the shearing rate, τ_L is the limiting shear stress of the lubricant, τ_{L0} is the initial shear stress of the lubricant, γ_L is the pressure coefficient corresponding to the maximum friction coefficient in hydrodynamic lubrication, and p_h is the fluid pressure. According to Bair et al. [4], for oil lubricant, τ_{L0} = 2MPa and γ_L = 0.05.

The thermal EHL problem defined through Equations S(1) to S(18) can be solved iteratively

through numerical methods to obtain lubrication performance parameters. The method of solving the system has been studied by researchers [1, 2, 5-8]. Here, we only address some key points in the solutions. In order to perform numerical solution procedures, equations are non-dimensionalized first.

The following dimensionless variables are used when solving the pressure distribution:

$$X=\frac{x}{a}, Y=\frac{y}{b}, H=\frac{hR_x}{a^2}, P=\frac{P}{p_h}, \overline{\eta}=\frac{\eta}{\eta_0}, \overline{\rho}=\frac{\rho}{\rho_0}$$

where a and b are the radius of Hertzian contact in two principal directions. In point contact, a equals b. p_h is the maximum Hertzian contact pressure value. R_x is the radius of curvature in the x direction, and η_0 and ρ_0 are, respectively, the ambient viscosity and density of the lubricant. The Hertzian contact parameters for point contact are calculated as follows

$$a=b=\left(\frac{3wR_x}{2E_e}\right)^{\frac{1}{3}}, \quad p_h=\frac{3w}{2\pi a^2} \tag{S(19)}$$

The non-dimensional form of the Reynolds equation is

$$\frac{\partial}{\partial X}\left(\varepsilon_x\frac{\partial P}{\partial X}\right)+\frac{\partial}{\partial Y}\left(\varepsilon_y\frac{\partial P}{\partial Y}\right)=\frac{\partial\left(\overline{\rho}H\right)}{\partial X}+\frac{\partial\left(\overline{\rho}H\right)}{\partial \overline{t}} \tag{S(20)}$$

where

$$\varepsilon_x=\varepsilon_y=\frac{a^3p_h}{12\eta_0u_sR_x^2}\frac{\overline{\rho}H^3}{\overline{\eta}}$$

$$u_s=\frac{u_1+u_2}{2}$$

$$\overline{t}=\frac{u_st}{a}$$

The non-dimensional film thickness equation is:

$$H\left(x,t\right)=\frac{h\left(x,t\right)R_x}{a^2}=H_{00}\left(t\right)+\frac{X^2}{2}+\frac{Y^2}{2}+\left[r\left(x,y,t\right)+v\left(x,y,t\right)\right]\frac{R_x}{a^2} \tag{S(21)}$$

The non-dimensional elastic deformation equation:

$$V=\frac{2}{\pi^2}\iint_{\Omega}\frac{P\left(\xi,\zeta\right)}{\sqrt{\left(X-\xi\right)^2+\left(Y-\zeta\right)^2}}d\xi d\zeta \tag{S(22)}$$

The non-dimensional load balance equation:

$$\frac{2\pi}{3}=\iint_{\Omega} P\left(X,Y,\bar{t}\right)dXdY \tag{S23}$$

The non-dimensional Reynolds equation, S(20), needs to be discretized for a numerical solution. The authors studied several different discrete methods [9]. Here the recommended discrete form is shown below.

$$\alpha_{i,j}^{(s)}P_{i-1,j}^{(s+1)}+\beta_{i,j}^{(s)}P_{i,j}^{(s+1)}+\gamma_{i,j}^{(s)}P_{i+1,j}^{(s+1)}=b_{i,j}^{(s)} \tag{S24}$$

where (s) denotes the iteration index, and $\alpha_{i,j}^{(s)}$, $\beta_{i,j}^{(s)}$, $\gamma_{i,j}^{(s)}$, and $b_{i,j}^{(s)}$ are the coefficients shown below.

$$\alpha_{i,j}^{(s)}=\varepsilon_{i-1/2,j}^{x(s)}-\left(\bar{\rho}_{i,j}^{(s)}D_{i-1,j}^{i,j}-\bar{\rho}_{i-1,j}^{(s)}D_{i-1,j}^{i,j}\right)\Delta X-\left(\bar{\rho}_{i,j}^{(s)}D_{i-1,j}^{i,j}-\bar{\rho}_{i,j}^{(s)}D_{i-1,j}^{i-1,j}\right)\Delta X-2\left(\bar{\rho}_{i,j}^{(s)}D_{i-1,j}^{i,j}\right)\Delta X^2\Big/\Delta\bar{t}$$

$$\beta_{i,j}^{(s)}=\begin{bmatrix}-\left(\varepsilon_{i-1/2,j}^{x(s)}+\varepsilon_{i+1/2,j}^{x(s)}+\varepsilon_{i,j-1/2}^{y(s)}+\varepsilon_{i,j+1/2}^{y(s)}\right)-\left(\bar{\rho}_{i,j}^{(s)}D_{i,j}^{i,j}-\bar{\rho}_{i,j}^{(s)}D_{i,j}^{i-1,j}+\bar{\rho}_{i,j}^{(s)}D_{i,j}^{i,j}-\bar{\rho}_{i-1,j}^{(s)}D_{i,j}^{i,j}\right)\Delta X\cdots\\ \cdots-2\left(\bar{\rho}_{i,j}^{(s)}D_{i,j}^{i,j}\right)\Delta X^2\Big/\Delta\bar{t}\end{bmatrix}$$

$$\gamma_{i,j}^{(s)}=\varepsilon_{i+1/2,j}^{x(s)}-\left(\bar{\rho}_{ij}^{(s)}D_{i+1,j}^{i,j}-\bar{\rho}_{i-1j}^{(s)}D_{i+1,j}^{i,j}\right)\Delta X-\left(\bar{\rho}_{ij}^{(s)}D_{i+1,j}^{i,j}-\bar{\rho}_{ij}^{(s)}D_{i+1,j}^{i-1,j}\right)\Delta X-2\left(\bar{\rho}_{ij}^{(s)}D_{i+1,j}^{i,j}\right)\Delta X^2\Big/\Delta\bar{t}$$

$$b_{i,j}^{(s)}=-\left(\varepsilon_{i,j-1/2}^{y(s)}P_{i,j-1}^{(s)}+\varepsilon_{i,j+1/2}^{y(s)}P_{i,j+1}^{(s)}\right)+\begin{bmatrix}\bar{\rho}_{ij}^{(s)}\left(H_{ij}^{(s)}-H_{i-1,j}^{(s)}\right)-\left(\bar{\rho}_{i,j}^{(s)}D_{i,j}^{i,j}-\bar{\rho}_{i,j}^{(s)}D_{i,j}^{i-1,j}\right)P_{ij}^{(s)}\\ -\left(\bar{\rho}_{i,j}^{(s)}D_{i-1,j}^{i,j}-\bar{\rho}_{i-1,j}^{(s)}D_{i-1,j}^{i,j}\right)P_{i-1,j}^{(s)}-\left(\bar{\rho}_{i,j}^{(s)}D_{i-1,j}^{i,j}-\bar{\rho}_{i,j}^{(s)}D_{i-1,j}^{i-1,j}\right)P_{i-1j}^{(s)}\end{bmatrix}\Delta X\cdots$$

$$\cdots+\begin{bmatrix}H_{ij}^{(s)}\left(\rho_{ij}^{(s)}-\rho_{i-1,j}^{(s)}\right)-\left(\bar{\rho}_{i,j}^{(s)}D_{i,j}^{i,j}-\bar{\rho}_{i-1,j}^{(s)}D_{i,j}^{i,j}\right)P_{ij}^{(s)}\\ -\left(\bar{\rho}_{ij}^{(s)}D_{i+1,j}^{i,j}-\bar{\rho}_{i-1j}^{(s)}D_{i+1,j}^{i,j}\right)P_{i+1,j}^{(s)}-\left(\bar{\rho}_{ij}^{(s)}D_{i+1,j}^{i,j}-\bar{\rho}_{ij}^{(s)}D_{i+1,j}^{i-1,j}\right)P_{i+1,j}^{(s)}\end{bmatrix}\Delta X\cdots$$

$$\cdots+\begin{bmatrix}H_{ij}^{(s)}\left(\bar{\rho}_{ij}^{(s)}-\bar{\rho}_{ij}^{(s-1)}\right)+\bar{\rho}_{ij}^{(s)}\left(H_{ij}^{(s)}-H_{ij}^{(s-1)}\right)\\ -2\bar{\rho}_{i,j}^{(s)}D_{i,j}^{i-1,j}P_{i-1,j}^{(s)}-2\bar{\rho}_{i,j}^{(s)}D_{i,j}^{i,j}P_{ij}^{(s)}-2\bar{\rho}_{i,j}^{(s)}D_{i,j}^{i-1,j}P_{i-1j}^{(s)}\end{bmatrix}\Delta X^2\Big/\Delta\bar{t}$$

The D represents the influence matrix derived from the non-dimensional elastic deformation equation, S(22), for calculating the elastic deformation. The discrete form of S(22) is

$$V_{i,j}=\sum_{k=1}^{M-1}\sum_{l=1}^{N-1}D_{k,l}^{i,j}P_{k,l} \tag{S25}$$

The expression of the influence matrix D can be found in the work of Liu et al. [10].

The dimensionless variables for solving the temperature distribution are as follows:

$$\bar{x}=x/a\ ,\quad \bar{y}=y/a\ ,\quad H=h/a\ ,\quad \bar{t}=t\cdot 4\alpha_s/l^2\ ,\quad \bar{V}=V\cdot l/\left(4\alpha_s\right)\ ,\quad \Delta\bar{T}=\Delta T\cdot\pi^{3/2}\rho_s c_s/\left(2p_h\right),$$

$$\bar{q}=q\cdot l/\left(4p_h\alpha_s\right)$$

The material of the two bodies is assumed to be the same.

The non-dimensional temperature rise equation is,

$$\Delta\overline{T}_1\left(X,Y,\overline{t}\right)=\int_0^{\overline{t}}\iint_{\Omega_q}\left\{\left[1-f\left(\overline{X}',\overline{Y}',\overline{t}'\right)\right]\overline{q}\left(\overline{X}',\overline{Y}',\overline{t}'\right)-\overline{q}_c\left(\overline{X}',\overline{Y}',\overline{t}'\right)\right\}\times\exp\left\{\frac{\left[\left(X-\overline{X}'\right)-U_1\left(\overline{t}-\overline{t}'\right)\right]^2+\left(Y-\overline{Y}'\right)^2}{\left(\overline{t}-\overline{t}'\right)}\right\}\times\frac{d\overline{X}'d\overline{Y}'d\overline{t}'}{\left(\overline{t}-\overline{t}'\right)^{3/2}} \quad \text{S(26)}$$

$$\Delta\overline{T}_2\left(X,Y,\overline{t}\right)=\int_0^{\overline{t}}\iint_{\Omega_q}\left\{f\left(\overline{X}',\overline{Y}',\overline{t}'\right)\overline{q}\left(\overline{X}',\overline{Y}',\overline{t}'\right)+\overline{q}_c\left(\overline{X}',\overline{Y}',\overline{t}'\right)\right\}\times\exp\left\{\frac{\left[\left(X-\overline{X}'\right)-U_2\left(\overline{t}-\overline{t}'\right)\right]^2+\left(Y-\overline{Y}'\right)^2}{\left(\overline{t}-\overline{t}'\right)}\right\}\times\frac{d\overline{X}'d\overline{Y}'d\overline{t}'}{\left(\overline{t}-\overline{t}'\right)^{3/2}} \quad \text{S(27)}$$

The non-dimensional matching equation of temperature is,

$$\left[\overline{T}_{2b}+\Delta\overline{T}_2\left(X,Y,\overline{t}\right)\right]-\left[\overline{T}_{1b}+\Delta\overline{T}_1\left(X,Y,\overline{t}\right)\right]=\frac{\left(1-2f\left(X,Y,\overline{t}\right)\right)H\left(X,Y,\overline{t}\right)\overline{q}\left(X,Y,\overline{t}\right)}{2K_f}-\frac{H\left(X,Y,\overline{t}\right)\overline{q}_c\left(X,Y,\overline{t}\right)}{K_f} \quad \text{S(28)}$$

The temperature rise equations, S(26) and S(27), can only be numerically calculated as follows

$$\Delta\overline{T}\left(m,n,p\right)=\sum_{k=1}^{p}\sum_{i=0}^{M}\sum_{j=0}^{N}C_{i,j,k}^{m,n,p}\times\overline{q}\left(i,j,k\right) \quad \text{S(29)}$$

where $C_{i,j,k}^{m,n,p}$ is the influence coefficient of temperature rise. It is defined as the temperature rise at point (m, n) and time t resulting from a unit heat source at point (i, j) during period k. The calculation of $C_{i,j,k}^{m,n,p}$ can refer to Liu et al. [1]

The discrete non-dimensional equations above are solved numerically. The corresponding solution flow chart is shown in Figure S.1. The outer loop is for the time step. At every time step, the discrete Reynolds equation S(24) is solved iteratively for the pressure distribution. For a specific j value, S(24) turns into a tridiagonal system, which can be easily solved by the Thomas method. The relative difference of pressure distributions from two adjacent iterations is used as the index to show the convergence of pressure distribution. The corresponding equation is,

$$\frac{\sum\sum\left|P^{(s+1)}-P^{(s)}\right|}{\sum\sum\left|P^{(s)}\right|}\le\varepsilon_P \quad \text{S(30)}$$

where ε_P is the threshold value, set as 1×10^{-6} in the current study. If equation S(30) is not satisfied, the pressure distribution is updated by the under-relaxation method as follows,

$$P_{ij}^{(s+1)} = P_{ij}^{(s)} + \left(1-\omega\right)P_{ij}^{(s)} \quad \text{S(31)}$$

where ω is the under-relaxation factor equaling 0.8 in the current study. Once equation S(30) is satisfied, the converged pressure distribution is used to calculate the load-carrying capacity. The relative error between the load-carrying capacity and the applied load is used to test the satisfaction of the load balance equation. The corresponding equation is

$$\frac{\sum\sum\left|W^{(s+1)} - W\right|}{\sum\sum W} \le \varepsilon_W \quad \text{S(32)}$$

where ε_W is the threshold value, set as 1×10^{-6} in the current study. W is the non-dimensional applied load, equal to $2\pi/3$ according to the non-dimensional load balance equation S(23). If equation S(32) is not satisfied, the film thickness distribution is adjusted with a specific value. According to the work of Wang et al. [11], the proportional integral derivative (PID) controller is used to calculate the adjustment value of film thickness distribution, ΔH, as follows,

$$\Delta H = K_p\left[e(s)-e(s-1)\right] + K_i e(s) + K_d\left[e(s)-2e(s-1)+e(s-2)\right] \quad \text{S(33)}$$

where K_p, K_i, and K_d are coefficients of the PID controller, $e(s)$, $e(s-1)$, and $e(s-2)$ are the absolute error between load-carrying capacity and the applied load at the iteration s, $s-1$, and $s-2$, respectively, e.g., $e(s) = W^{(s)}-W$. In the current study, K_p equals 0.01, K_i equals 0.005, and K_d equals zero.

Once equation S(32) is satisfied, the shear stress is calculated and the solution moves into the temperature loop. The heat partition coefficients, additional heat flux, and surface temperature distributions are solved iteratively. Detailed algorithms can refer to Liu et al. [1, 2]. The relative difference of average temperature distributions from two adjacent iterations is used as the index to show the convergence of temperature distribution. The corresponding equation is,

$$\frac{\sum\sum\left|T_{avg}^{(s+1)} - T_{avg}^{(s)}\right|}{\sum\sum\left|T_{avg}^{(s)}\right|} \le \varepsilon_T \quad \text{S(34)}$$

where ε_T is the threshold value, set as 1×10^{-4} in the current study. If equation S(34) is not satisfied, the average temperature distribution is updated by the under-relaxation method as follows,

$$T_{avg}^{(s+1)} = T_{avg}^{(s)} + \omega_T\left(T_{avg}^{(s+1)} - T_{avg}^{(s)}\right) \quad \text{S(35)}$$

where ω_T is the under-relaxation factor equaling 0.3 in the current study.

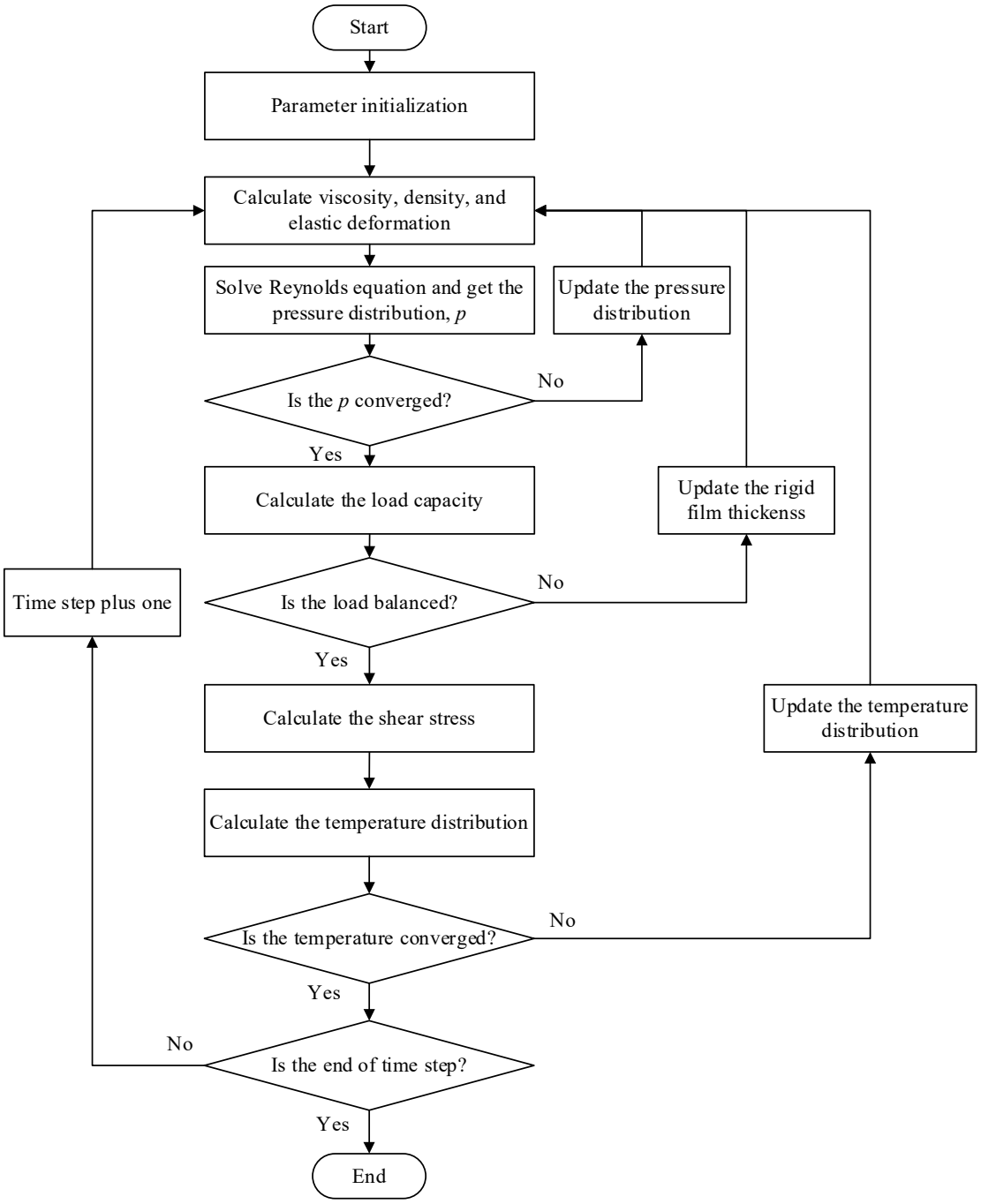

Figure S.1 Flow chart of the numerical solution procedures

Once equation S(34) is satisfied, the solution moves to next time step. Accordingly, the surface roughness has to be cyclically shifted a certain distance in the relative movement direction of the two mating surfaces. Theoretically, the moving distance is determined by the time interval and the relative speed. However, it is always set as an integer multiple space interval of the solution domain in numerical simulation to simplify the programming. After updating the roughness, the pressure and temperature distributions are solved again, as described above. The solution procedures will stop once the predefined end-time value is reached.

2 Results

2.1 Model validation

The transient TEHL model is validated with the experimental results of He et al. [3]. Specifically, the experimental results shown in one sub-figure of Figure 8 in their paper are extracted. The sub-figure used is indexed with 'Load: 500N'. Most simulation parameters are the same as reported in Ref [10] except for the roughness data. He et al. [3] used measured roughness but did not provide it. Thus, we use numerically generated Gaussian surfaces instead. The root-mean-square roughness is set equaling that of Ref [10]. Figure S.2 shows the coefficient of friction (COF) simulated with the model and codes in this work and those extracted. The simulated COF matches well with the experimental ones, validating the model and codes in this work.

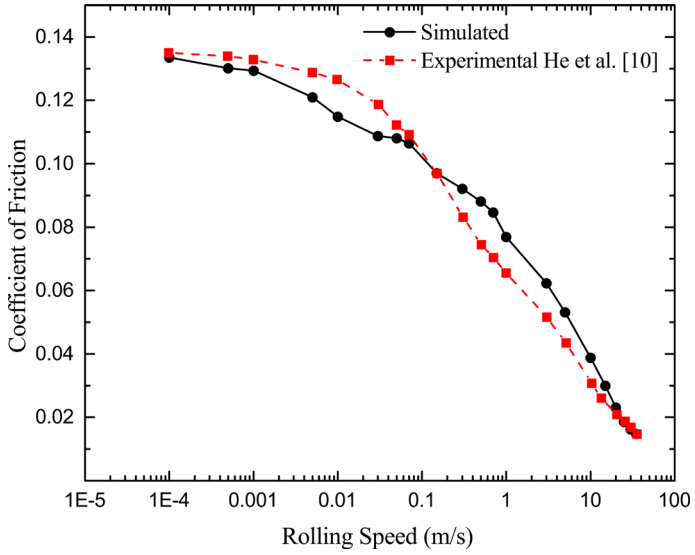

Figure S.2 Model validation with experimental results of He et al. [10]

The convergence of the transient TEHL is illustrated with the evolution of minimum film thickness and maximum pressure along with time. Without losing generality, the results with w = 200N, u_s = 3m/s, θ = 0°, A = 0.09 , and $\Omega_x \approx 39.8$ (N_w = 19) are used. Figure S.3 and Figure S.4 show the change in minimum film thickness and maximum pressure as the time step increases, respectively. The results suggest that the minimum film thickness and maximum pressure approach stable values, fluctuating periodically as the time step increases.

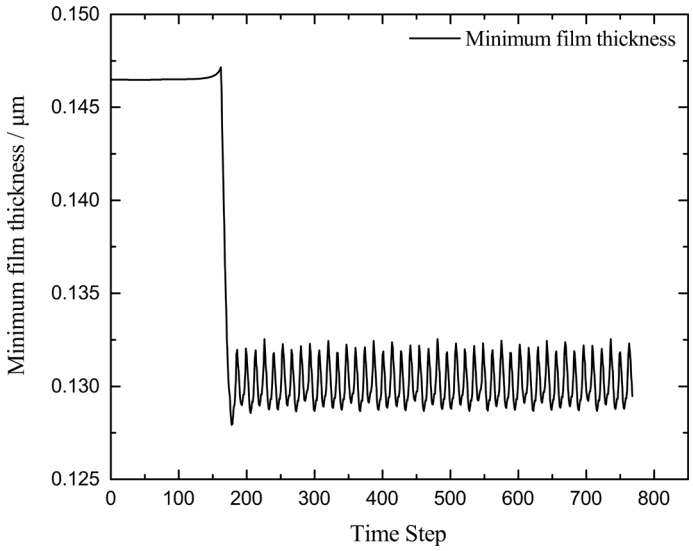

Figure S.3 The minimum film thickness at each time step for selected working parameters

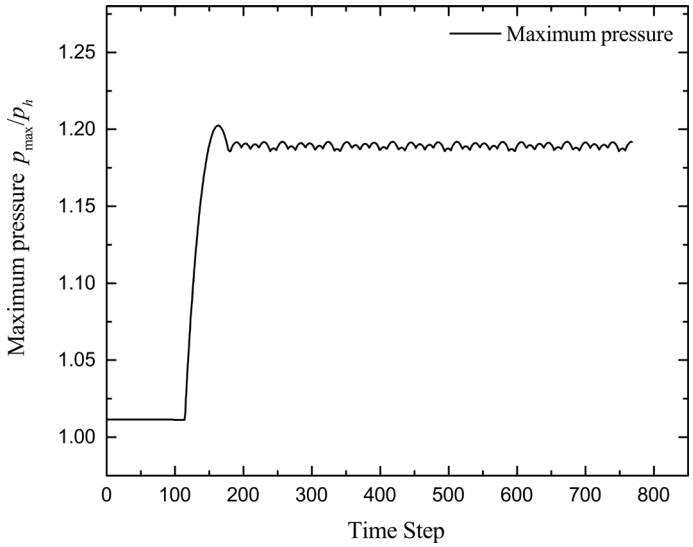

Figure S.4 The maximum pressure at each time step for selected working parameters

2.2 Grid convergence study

In order to test the grid convergence of the selected grid density, 256×256, three different grid densities, 256×256, 512×512, and 1024×1024, are used to simulate the steady-state EHL case with $N_w = 32$, $A = 0.3$, $\theta = 0°$, $w = 200$N, and $u_s = 3$m/s. The combination of $N_w = 32$ and $A = 0.3$ results in the most significant non-dimensional waviness used in the current study. Considering the non-dimensionalization of waviness (equations 6 to 8 in the paper), the working conditions with a large central film thickness and smaller Hertzian contact zone result in more significant dimensional waviness. The working condition satisfying this condition is $w = 200$N and $u_s = 3$m/s in this work. Therefore, the parameters used for the grid convergence study ensure that the most significant waviness is tested. The central lines of the film thickness and pressure distributions are shown in

Figure S.5. The results show that increasing the grid density from 256×256 to 1024×1024 only causes slight differences. In the meantime, using coarse grids can save a considerable amount of computational resources, especially dealing with transient Reynolds equations and a large parameter matrix of simulation. Therefore, the current study sticks with the grid density of 256×256.

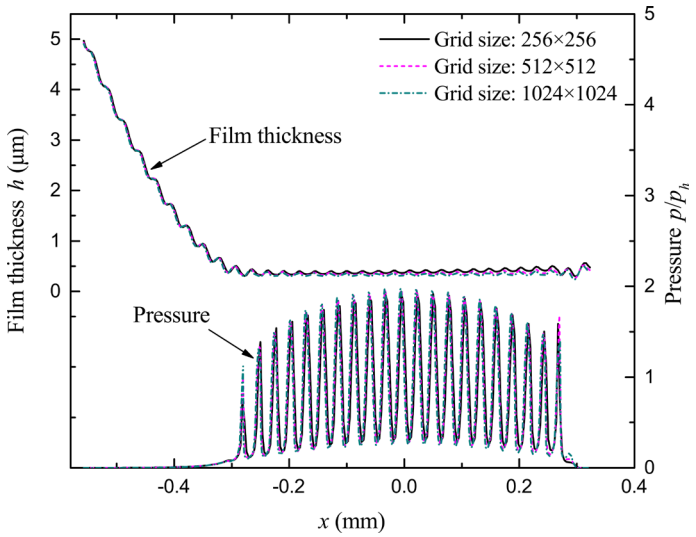

Figure S.5 The central lines of the film thickness and pressure distributions with different grid densities.

2.3 Contour maps

Supplemental Material S2 is a zip file containing all contour maps and simulated data.

Reference:

[1] Liu YC, Wang H, Wang WZ, Hu YZ, Zhu D. Methods comparison in computation of temperature rise on frictional interfaces. Tribology International. 2002;35:549-60.

[2] Liu YC, Hu YZ, Wang WZ, Wang H. Simulation of temperature distribution of point, contacts in mixed lubrication. Science in China Series E-Technological Sciences. 2002;45:365-72.

[3] He T, Zhu D, Wang J, Jane Wang Q. Experimental and Numerical Investigations of the Stribeck Curves for Lubricated Counterformal Contacts. Journal of Tribology. 2016;139.

[4] Bair S, Winer WO. The high pressure high shear stress rheology of liquid lubricants. Journal of Tribology. 1992;114:1-9.

[5] Ai X. Numerical analyses of elastohydrodynamically lubricated line and point contacts with rough surfaces by using semi-system and multigrid methods. (Volumes I and II): Northwestern University.; 1993.

[6] Lubrecht AA, ten Napel WE, Bosma R. Multigrid, An Alternative Method for Calculating Film

Thickness and Pressure Profiles in Elastohydrodynamically Lubricated Line Contacts. Journal of TribologyJournal of Tribology. 1986;108:551.

[7] Venner CH, Lubrecht AA. Numerical Analysis of the Influence of Waviness on the Film Thickness of a Circular EHL Contact. Journal of Tribology. 1996;118:153.

[8] Huang P. Numerical calculation of lubrication: methods and programs: John Wiley & Sons; 2013.

[9] Wang YC, Dorgham A, Liu Y, Wang C, Wilson MCT, Neville A, et al. An Assessment of Quantitative Predictions of Deterministic Mixed Lubrication Solvers. Journal of Tribology-Transactions of the ASME. 2021;143:011601.

[10] Liu SB, Wang Q, Liu G. A versatile method of discrete convolution and FFT (DC-FFT) for contact analyses. WEAR. 2000;243:101-11.

[11] Wang Y, Liu Y, Wang Y. A method for improving the capability of convergence of numerical lubrication simulation by using the PID controller. Advances in Mechanism and Machine Science: Springer Netherlands; 2019. p. 3845-54.